



## Protonation of Imino Moiety in Aminoguanidine by Heterolytic O–H Bond Cleavage on Phthalic Acid: Theoretical, Experimental and DNA Binding Studies

L. RAJASEKAR<sup>✉</sup>, R. RAJESH, D. DILEEP, R. PRADEEP and B.N. SIVASANKAR<sup>\*✉</sup>

Department of Chemistry, Government Arts College, Udthagamandalam-643002, India

\*Corresponding author: E-mail: sivabickol@yahoo.com

Received: 4 November 2022;

Accepted: 8 December 2022;

Published online: 30 January 2023;

AJC-21123

Aqueous neutralization reaction between aminoguanidine hydrogencarbonate and phthalic acid yielded the crystals of aminoguanidine hydrogenphthalate monohydrate (AHPMH). The crystal quality is further improved by repeated recrystallization and single crystals were obtained. The single crystal XRD data reveals that the compound crystallizes in the monoclinic crystal system with the *Cc* space group. The unit cell consists of four molecules ( $z = 4$ ) and in the crystal lattice they are linked by O–H...O and N–H...O intermolecular hydrogen bonding. Geometrical and vibrational analyses were performed by B3LYP/6311G(d,p) basis set and compared with the single crystal XRD values. The Mulliken charge and molecular electrostatic potential (MEP) analyses have been used to predict the reaction behaviour and bond cleavage fashion during the reaction. The heterolytic O-H bonding electrons are shifted towards the oxygen atom (-0.6112 e) and it possesses high electronegative which influenced the formation of strong hydrogen bond. The binding constant ( $K_b$ ) of the AHPMH indicates that strong interactions are developed between the title compound and CT-DNA.

**Keywords:** Aminoguanidine, X-ray diffraction, Elecrofuge leaving group, Heterolytic O-H bond fission, HOMO-LUMO.

### INTRODUCTION

Proton transfer reactions play a vital role in several biological and chemical processes [1,2]. Ground state electron transfer reactions are an elementary and crucial process found in chemical science and they have an excellent role in chemical physics. Protonation consists of three steps (i) donor moieties and acceptor moieties find each other in a chemical environment (ii) the electronic cloud of hydrogen (H) arrives to the electronegative donor to form a covalent bond (iii) the acceptors acquire lone-pair of electrons. Molecules involving excited state intramolecular proton transfer (ESIPT) have a great technological significance like (UV) stabilizers [3], tunable lasers [4], for optical switching and information storage [5].

Aminoguanidine (AG) is considered as a nitrogenated analogous of ureas and amides. Nevertheless, its distinctive structure generates them the compound of enormous basicity, very similar to amines than amides [6,7]. Aminoguanidine and guanidine derivatives have found applications in both biological and chemical systems [8,9]. The chemical physiological and biological properties of AG derivatives has been ascribed

to their strong basicity [10-13]. Indeed, aminoguanidine and derivatives commonly prevent diabetic complications such as retinopathy and angiopathy [14,15]. The compound having a carbonohydraxonic diamide group is known for its anti-leukemia activity [16].

Solvent system concept suggests all acids and bases are stronger than the characteristic cation and the anion of the solvent would be leveled to the characteristic cation and anion of the solvents. Acids and bases weaker than the characteristic cation and anion of the solvent would remain in equilibrium with them. Studies on solvent effects on proton transfer reactions are abetted to understand the factors that are responsible for the relatively high energy barriers in these reactions [17-19].

Protonated form of aminoguanidine (AG) has found extensive application in the medicinal fields over the last two decades [20], which motivated the investigation of aminoguanidinium salt of carboxylates. In present study, an attempt has been made to report synthesize, structure determination and DFT studies on aminoguanidine hydrogenphthalate monohydrate (AHPMH). Studies on DNA binding have also been conducted, and the outcomes are reviewed in detail.

## EXPERIMENTAL

The chemicals and solvents were purchased from HiMedia Pvt. Ltd., India. The double distilled water was used throughout the studies. The elemental (C, H and N) contents were determined by using Perkin-Elmer 2400 series elemental analyzer. IR spectra of aminoguanidine hydrogenphthalate monohydrate (AHPMH) and phthalic acid were recorded on Bruker Alpha spectrometer (KBr pellet, 4000–400  $\text{cm}^{-1}$ ). The simultaneous TG-DTA measurement was performed by heating the sample from 400 to 800 K at a rate of 10 K  $\text{min}^{-1}$  in open air on SWI TG/DTA 6200 thermal analyzer using about 5 mg of sample using platinum cup as sample holder.

**Synthesis of aminoguanidine hydrogenphthalate monohydrate (AHPMH):** Aminoguanidine hydrogenphthalate monohydrate (AHPMH) was synthesized by the reaction between a hot aqueous solution of aminoguanidine hydrogen carbonate (0.01 mol, 1.36 g) and an aqueous solution of phthalic acid (0.01 mol, 1.66 g) (**Scheme-I**). The resulting turbid solution was stirred well to obtain clear solution and then filtered. The colourless filtrate was kept at room temperature for crystallization. A colourless needle-like single crystals of AGHMP formed after 48 h were collected, washed with distilled water and dried in air. The crystals were further purified by recrystallization from distilled water. Yield: 77%. Anal. calcd. (found) %: C, 41.85 (42.56); H, 5.46 (5.02); N, 21.69 (22.46);  $\text{N}_2\text{H}_4$ , calcd. 12.39%, Found 11.64%.

**X-ray crystallographic studies:** Single crystal X-ray data collection was carried out with Bruker AXS Kappa Apex II CCD diffractometer equipped with graphite monochromated  $\text{MoK}\alpha$  ( $\lambda = 0.71073 \text{ \AA}$ ) radiation. The intensity data for the structure determination were collected through an optimized strategy, which gives an average 4-fold redundancy. The program, APEX2-SAINT [21] was used for integrating the frames. Four-fold redundancy per reflection was utilized for achieving good multi-scan absorption correction using SADABS program [21]. Besides absorption, Lorentz, polarization and decay corrections were applied to intensity during data reduction. The structure was solved by direct methods using SIR92 [22] and refined by full-matrix least squares techniques using SHELXL-2014 program [23,24].

**Computational studies:** Density functional theory (DFT) calculations were carried out using Gaussian 16 software [25]. All the molecular structures are visualized using Gaussview 06 software package. The vibrational frequency analysis and optimization geometry of aminoguanidine (AG), phthalic acid and AHPMH were done by B3LYP [26,27] level of theory with 6-311G(d,p) [28,29] basis set. Mulliken charge analysis

plays an important role in proton transfer reaction and also done by the same basis level and basis set.

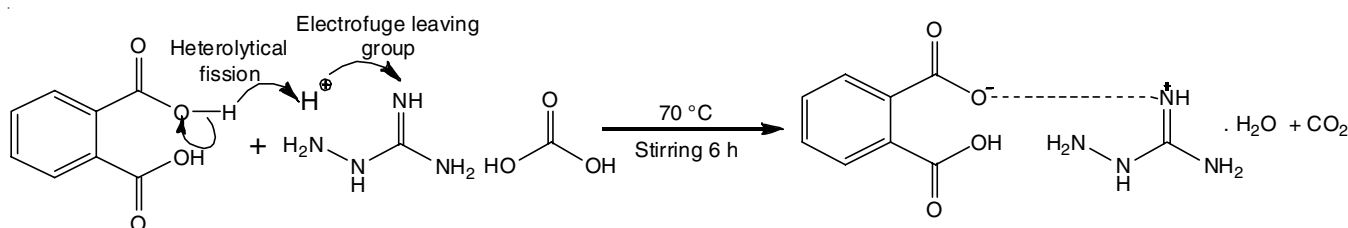
**DNA binding studies:** Intercalation binding study of AHPMH with calf thymus DNA (CT-DNA) was carried out in a buffer containing 50 mmol of NaCl adjusted to pH 7.2 with tris-HCl. A solution of CT-DNA gave a ratio of UV absorbance of about 1.8–1.9 at 250 and 260 nm. This indicates that CT-DNA was sufficiently free of protein. The CT-DNA concentration was determined from its extinction coefficient value 6600  $\text{M}^{-1} \text{cm}^{-1}$  at 260 nm.

## RESULTS AND DISCUSSION

**Crystal structure:** Aminoguanidine hydrogenphthalate monohydrate (AHPMH) crystallizes in the monoclinic crystal system with  $Cc$  space group having  $z = 4$ . The crystallographic details and refinement data are given in Table-1. Bond lengths

TABLE-1  
CRYSTAL DATA AND STRUCTURE REFINEMENT FOR AGHP

Identification code	AHPMH
Empirical formula	$\text{C}_8\text{H}_{14}\text{N}_4\text{O}_5$
Formula weight	258.24
Temperature	293(2) K
Wavelength	0.71073 $\text{\AA}$
Crystal system	Monoclinic
Space group	$Cc$
Unit cell dimensions	$a = 7.6608(3) \text{ \AA}$ ; $\alpha = 90^\circ$ $b = 13.6239(7) \text{ \AA}$ ; $\beta = 94.615(2)^\circ$ $c = 11.2041(4) \text{ \AA}$ ; $\gamma = 90^\circ$
Volume	1165.58(9) $\text{\AA}^3$
Z	4
Density (calculated)	1.472 $\text{Mg/m}^3$
Absorption coefficient	0.121 $\text{mm}^{-1}$
F(000)	544
Crystal size	0.250 × 0.200 × 0.200 $\text{mm}^3$
$\theta$ range for data collection	2.990 to 27.998°
Index ranges	$-10 \leq h \leq 10$ , $-17 \leq k \leq 17$ , $-14 \leq l \leq 14$
Reflections collected	13376
Independent reflections	2808 [R(int) = 0.0193]
Completeness to $\theta = 25.242^\circ$	100.0 %
Absorption correction	Semi-empirical from equivalents
Max. and min. transmission	0.986 and 0.968
Refinement method	Full-matrix least-squares on $F^2$
Data/restraints/parameters	2808/15/200
Goodness-of-fit on $F^2$	1.051
Final R indices [ $I > 2\sigma(I)$ ]	R1 = 0.0304, wR2 = 0.0801
R indices (all data)	R1 = 0.0361, wR2 = 0.0861
Absolute structure parameter	0.3(2)
Extinction coefficient	0.0073(17)
Largest diff. peak and hole	0.219 and -0.216 $\text{e. \AA}^{-3}$



**Scheme-I:** Protonation of aminoguanidine by heterolytic O–H bond fission followed by electrofuge leaving group abstraction

and bond angles along with the theoretical values are listed in Table-2. The asymmetric unit of AHPMH salt consists of one monoprotonated cation (aminoguanidium), one anion (hydrogen

phthalate) and one water molecule. In the aminoguanidium moiety, three types of C-N bond lengths (Fig. 1a) exist in C(9), 1.323 Å, 1.319 Å and 1.308 Å for C(9)-N(2), C(9)-N(3) and

TABLE-2  
BOND LENGTHS AND BOND ANGLES ALONG WITH THEORETICAL VALUES

	Bond lengths (Å)		Bond angles (°)	
	Experimental	B3LYP/6311G(d,p)	Experimental	B3LYP/6-311G(d,p)
C(1)-C(2)	1.388(3)	1.402	C(2)-C(1)-C(6)	119.3(2)
C(1)-C(6)	1.402(2)	1.407	C(2)-C(1)-C(8)	118.86(18)
C(1)-C(8)	1.498(3)	1.489	C(6)-C(1)-C(8)	121.57(19)
C(2)-C(3)	1.382(4)	1.399	C(3)-C(2)-C(1)	120.5(2)
C(2)-H(2)	0.93	1.082	C(3)-C(2)-H(2)	119.7
C(3)-C(4)	1.371(4)	1.395	C(1)-C(2)-H(2)	119.7
C(3)-H(3)	0.93	1.08	C(4)-C(3)-C(2)	120.3(2)
C(4)-C(5)	1.386(4)	1.397	C(4)-C(3)-H(3)	119.9
C(4)-H(4)	0.93	1.082	C(2)-C(3)-H(3)	119.9
C(5)-C(6)	1.385(3)	1.396	C(3)-C(4)-C(5)	119.9(2)
C(5)-H(5)	0.93	1.082	C(3)-C(4)-H(4)	120.1
C(6)-C(7)	1.496(3)	1.508	C(5)-C(4)-H(4)	120.1
C(7)-O(2)	1.241(3)	1.273	C(6)-C(5)-C(4)	120.7(2)
C(7)-O(1)	1.264(3)	1.3	C(6)-C(5)-H(5)	119.7
C(8)-O(3)	1.222(3)	1.245	C(4)-C(5)-H(5)	119.7
C(8)-O(4)	1.287(3)	1.367	C(5)-C(6)-C(1)	119.3(2)
C(9)-N(4)	1.308(4)	1.34	C(5)-C(6)-C(7)	118.23(17)
C(9)-N(3)	1.319(4)	1.343	C(1)-C(6)-C(7)	122.2(2)
C(9)-N(2)	1.323(3)	1.355	O(2)-C(7)-O(1)	124.3(2)
N(1)-N(2)	1.401(3)	1.42	O(2)-C(7)-C(6)	118.35(19)
N(1)-H(1A)	0.84(2)	1.024	O(1)-C(7)-C(6)	117.28(19)
N(1)-H(1B)	0.86(2)	1.01	O(3)-C(8)-O(4)	123.7(2)
N(2)-H(2A)	0.84(2)	1.026	O(3)-C(8)-C(1)	121.53(19)
N(3)-H(3A)	0.82(2)	1.01	O(4)-C(8)-C(1)	114.66(18)
N(3)-H(3B)	0.82(2)	1.026	N(4)-C(9)-N(3)	121.2(3)
N(4)-H(4B)	0.83(2)	1.002	N(4)-C(9)-N(2)	120.0(2)
N(4)-H(4C)	0.83(2)	1.009	N(3)-C(9)-N(2)	118.8(3)
O(4)-H(4A)	0.82	0.978	N(2)-N(1)-H(1A)	114(3)
O(5)-H(5A)	0.88(2)	1.03	N(2)-N(1)-H(1B)	106(3)
O(5)-H(5B)	0.88(2)	0.966	H(1A)-N(1)-H(1B)	107(3)
			C(9)-N(2)-N(1)	119.6(2)
			C(9)-N(2)-H(2A)	111(2)
			C(9)-N(3)-H(3A)	121(3)
			C(9)-N(3)-H(3B)	119(3)
			H(3A)-N(3)-H(3B)	120(3)

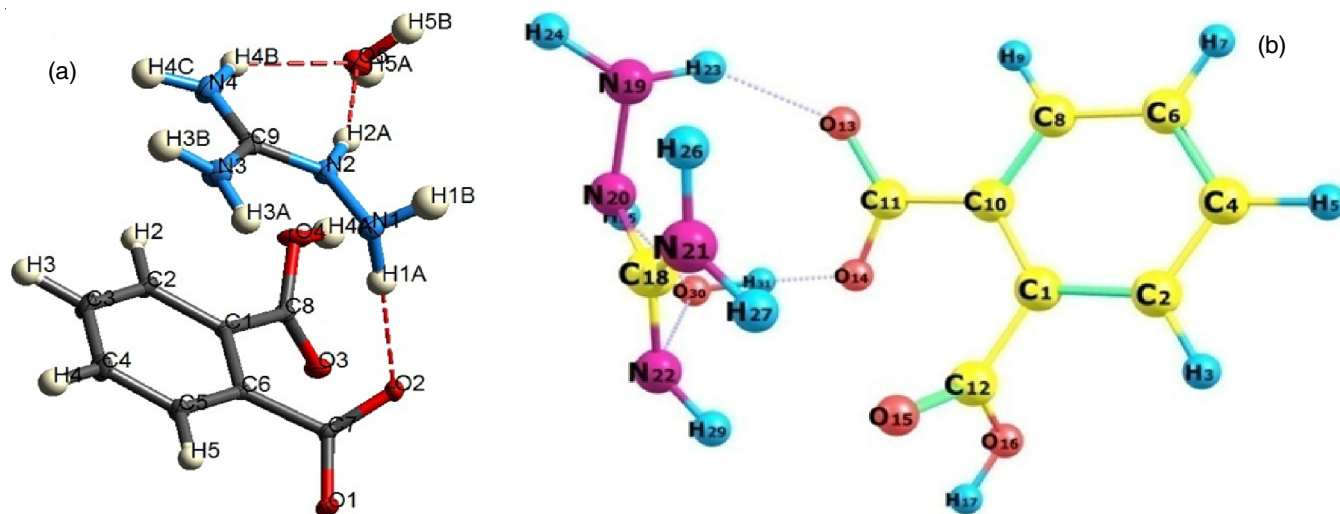


Fig. 1. Structure of AHPMH (a) thermal ellipsoid (30%) (b) theoretically optimized geometry

C(9)–N(4), respectively, indicating the partial double bond character between the carbon and nitrogen generates a resonance structure (Fig. 2). Usually, lone pair electrons on amino nitrogen atoms of aminoguanidine are associated in the  $\pi$ -system, which indicates to planar geometry over the amino nitrogen atoms. The central carbon atom (C9) of aminoguanidinium is bonded to three nitrogen atoms and its bond angles are  $121.33^\circ$  ( $\angle$ N(4)–C(9)–N(3)),  $120.0^\circ$  ( $\angle$ N(4)–C(9)–N(2)) and  $118.8^\circ$  ( $\angle$ N(3)–C(9)–N(2)) indicating almost trigonal planar geometry. Protonation appears particularly at imino nitrogen atom which indicates to a decrease in N(1)–N(2) (hydrazine) bond length (1.401 Å) and increase imino, C=N (C9–N2) double bond length (1.323 Å).

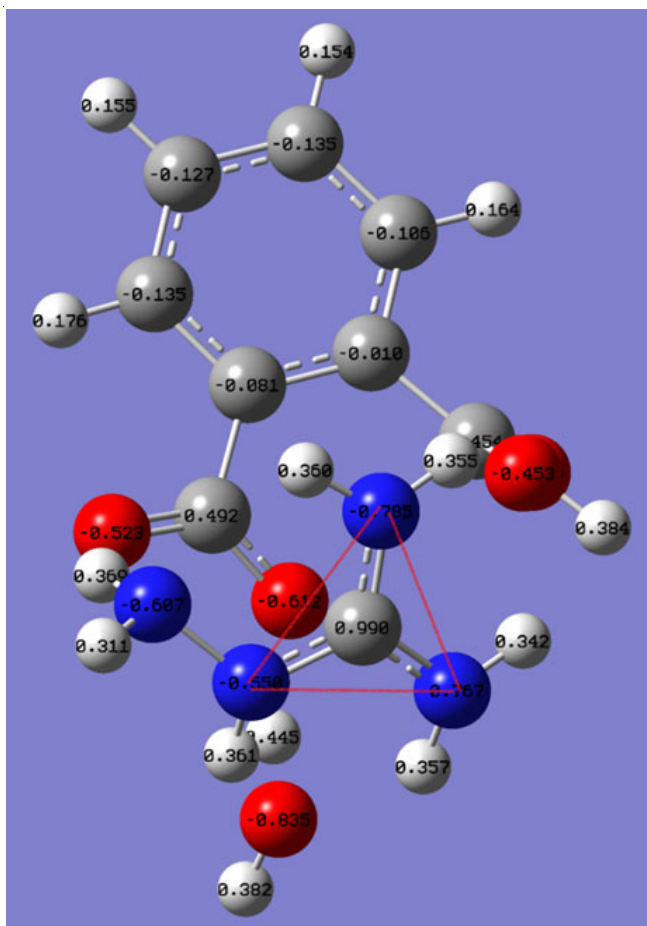


Fig. 2. Planar geometry due to the (C–N partial double bond nature) resonance

In the crystal structure, molecules are connected by intermolecular interactions and short contacts. The hydrogen bonding data are given in Table-3. The common intermolecular interactions observed in AHPMH are N–H...O and O–H...O (Fig. 1). N2–H2A...O5 and N4–H4B...O5 intermolecular hydrogen bonds combine the aminoguanidinium moiety (N9...H4B) with water. N1–H1A...O2 intermolecular interaction indicates that the (cation and anion connectivity) connection between aminoguanidinium (N1...H1) and hydrogen phthalate moiety. The O5–H5A...O2 and O5–H5B...O3 intermolecular hydrogen bonds connect the water (O5...H5A/H5B) with carboxylic acid and carboxylate moieties, respectively. Water molecule interacts

TABLE-3  
HYDROGEN BONDS FOR AGHP (Å and  $^\circ$ )

D–H...A	d(D–H)	d(H...A)	d(D...A)	$\angle$ (DHA)
O(4)–H(4A)...O(1)#1	0.82	1.67	2.488(2)	175.1
N(1)–H(1A)...O(2)	0.84(2)	2.24(2)	3.088(3)	177(3)
N(1)–H(1B)...O(1)#2	0.86(2)	2.36(3)	3.113(3)	147(4)
N(2)–H(2A)...O(5)	0.84(2)	2.03(3)	2.847(3)	165(3)
N(3)–H(3A)...O(4)#3	0.82(2)	2.60(3)	3.137(3)	124(3)
N(3)–H(3B)...O(2)#4	0.82(2)	2.15(3)	2.915(3)	156(4)
N(4)–H(4B)...O(5)	0.83(2)	2.31(3)	2.999(4)	141(3)
N(4)–H(4C)...O(3)#4	0.83(2)	2.22(2)	3.025(4)	164(4)
O(5)–H(5A)...O(2)#1	0.88(2)	1.90(2)	2.784(2)	174(4)
O(5)–H(5B)...O(3)#2	0.88(2)	1.97(3)	2.838(3)	171(4)

Symmetry transformations used to generate equivalent atoms:  
#1 x-1/2,-y+3/2,z-1/2 #2 x-1,y,z #3 x,-y+1,z+1/2 #4 x-1/2,y-1/2,z

with the cation through N2–H2A...O5 ( $D...A = 2.847$  Å and  $\angle D-H...A = 165^\circ$ ) and N4–H4B...O5 ( $D...A = 2.999$  Å) and  $\angle D-H...A = 141^\circ$ ) among these two interactions, former (N2–H2A...O5) is comparatively strong. Same water molecule also interacts with anion through O5–H5B...O3 ( $D...A = 2.838$  Å and  $\angle D-H...A = 171^\circ$ ). Thus, water molecule in the compound acts as hydrogen bond donor as well as hydrogen bond acceptor. The cation-anion intermolecular interaction (N1–H1...O2) is facilitating the strong ( $D...A = 3.088$  Å) connection between aminoguanidinium and hydrogen phthalate moieties and leads to stable crystal packing and this hydrogen bond is almost linear ( $D-H...A = 177^\circ$ ). The  $\pi$ - $\pi$  interactions are observed and the compound also involved in a steric crowding of N–H... $\pi$  interaction with carbonyl groups (Fig. 3). These groups of the imides provide extra stability to self-assemblies by participating in the weak interaction.

The comparison of experimental and theoretical parameters, bond lengths and bond angles are given in Table-2. The optimized molecular structure merges well with the solid state structure. The elimination of proton from the carboxylic acid group created remarkable changes in the net negative charge over the hydroxyl oxygen atom. The net negative charge increased due to heterolytic fission of the O–H bond. The bonding electron pairs in O–H bond are shifted towards the oxygen atom and it possesses high electronegativity which influenced the formation of strong hydrogen bonding interaction.

**FT-IR spectral analysis:** The vibrational frequency is carried out using B3LYP/6311+G(d,p) basis set. AHPMH consists of 32 atoms, which have 90 normal modes of vibrations. The complete vibrational assignments of the experimental wavenumbers are based on normal mode analyses and comparison with the theoretical scale values. The experimentally obtained IR spectrum of AHPMH is shown in Fig. 4 and some important frequency modes along with the calculated values are given in Table-4. The correlation between the theoretical and experimental results (Fig. 5) were  $R^2 = 0.093$ , which show the well-sufficient precision.

### Phenyl ring vibrations

**C–H vibrations:** The experimental IR spectrum shows C–H stretching frequencies in the region  $3220$ – $3160$   $\text{cm}^{-1}$ . The phenyl ring in AG molecule is bisubstituted and shows four aromatic C–H vibrations (C2–H3, C4–H5, C6–H7 and C8–H9).

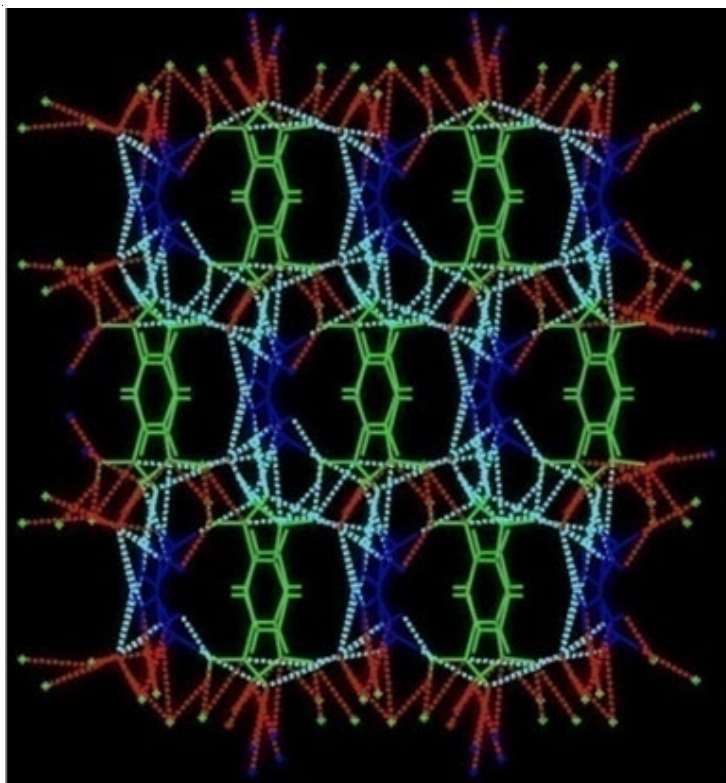
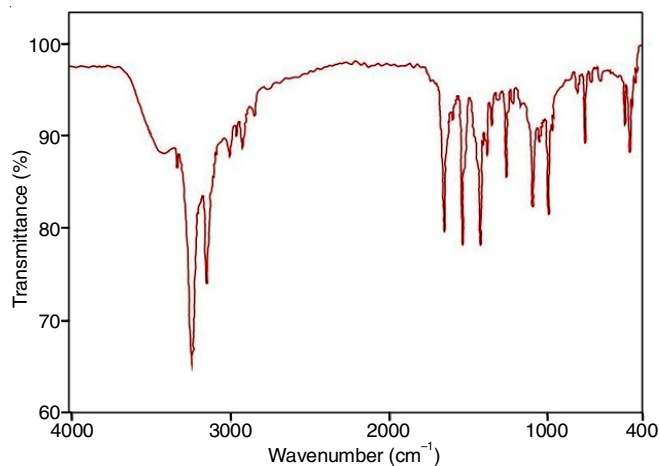
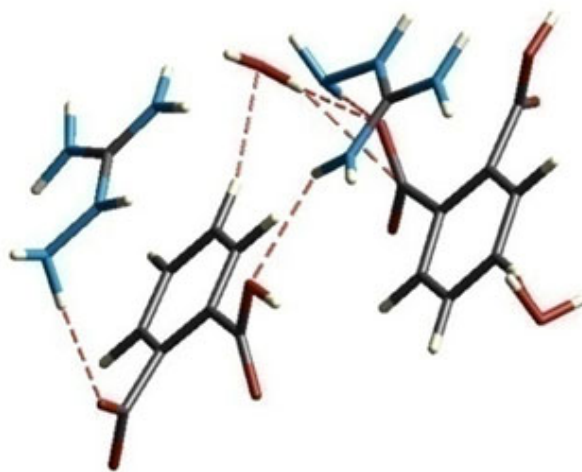
Fig. 3. 3D framework of N-H... $\pi$  interaction along with *c*-axis

Fig. 4. Experimental FT-IR spectrum of AHPMH

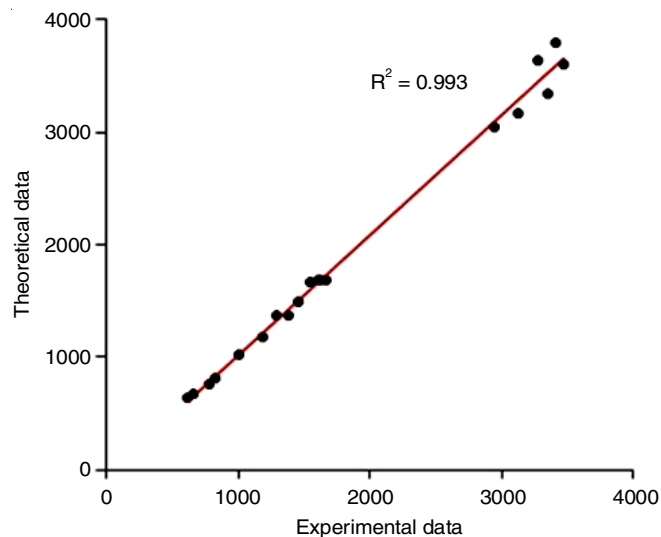


Fig. 5. Correlation between experimental and calculated IR frequencies

Theoretically, the charge on the atoms plays an important role in bond length, bond strength, dipole moment as well as the vibrational frequencies. The aromatic C-H stretching frequencies of AHPMH are slightly increased due to the resonance (charge variation on C and H atoms) within the carboxylate moiety. The calculated C-H stretching vibrational bands were observed at 3209, 3194, 3179 and 3167  $\text{cm}^{-1}$ . This apparently described increased electron density inside the phenyl ring due to charge transfer (CT) from an electron donor (AG) to acceptor (phthalic acid). The calculated C-H out-of-plane bending vibrations appeared at 996, 992, 809 and 805  $\text{cm}^{-1}$ .

**C-C vibrations:** The stretching vibrations of the aromatic ring are more valuable in the IR spectrum of benzene and its derivatives. These derivatives usually observed in the range

1650-1400  $\text{cm}^{-1}$  for stretching modes [30]. In AHPMH, the calculated C-C stretching vibrations were assigned at 1552, 1488 and 1334  $\text{cm}^{-1}$  and the difference between experimental (1470  $\text{cm}^{-1}$ ) and theoretical C-C stretching vibrations are in good agreement.

**Carboxylate ion ( $\text{COO}^-$ ) vibrations:** The strong band observed at 1660  $\text{cm}^{-1}$  and 1390  $\text{cm}^{-1}$  are due to the asymmetric and symmetric stretching vibrations, respectively of carboxylate ion. The theoretically calculated values appeared at 1665  $\text{cm}^{-1}$  and 1376  $\text{cm}^{-1}$ . The carbonyl frequency of free acid usually occurs at 1760-1730  $\text{cm}^{-1}$  which is completely vanished in AHPMH and this phenomenon supports the deprotonation of carboxylic

TABLE-4  
COMPARISON OF EXPERIMENTAL AND THEORETICAL VIBRATIONAL WAVENUMBERS OF AGH

Experimental wavenumbers (cm <sup>-1</sup> )	Calculated wavenumbers (cm <sup>-1</sup> ) (B3LYP/6311G (d,p))	Vibrational assignments
3420	3796	Free O-H vibration
3290	3631	Carboxylic acid O-H vibration
1630	1681	O-H-O in plane bending vibration
3480	3617, 3596, 3541	NH <sub>2</sub> assymetric stretching vibrations
790	769, 761, 723, 646	NH <sub>2</sub> out-of-plane bending vibrations
1290	1368	NH <sub>2</sub> wagging deformation
3360	3396, 3344	NH <sub>2</sub> symmetric stretching vibrations
1610	1694	N-H bending deformation for NH <sub>2</sub>
2960	3040	NH <sub>2</sub> <sup>+</sup> stretching vibration
3130	3209, 3194, 3179, 3167	Aromatic C-H stretching vibrations
1190	1212, 1176, 1130, 1031	Aromatic C-H in plane bending vibrations
830	996, 922, 809, 805	Aromatic C-H out-of-plane bending vibrations
1470	1522, 1488, 1334	Aromatic C-C stretching vibrations
1560	1665	COO <sup>-</sup> assymmetric stretching vibration
1390	1376, 1357	COO <sup>-</sup> symmetric stretching vibrations
670	680	COO <sup>-</sup> wagging vibration
620	639	COO <sup>-</sup> rocking vibration
1670	1540, 1681, 1657	C=N stretching vibrations
1130, 1005	1252, 1025	N-N stretching vibrations

acid group. The experimentally obtained bands at 670 and 620 cm<sup>-1</sup> were assigned for COO<sup>-</sup> wagging and rocking vibration modes, respectively and their theoretical values are shown in Table-4.

**O-H vibrations:** From the experimental spectrum, the identification of carboxylic acid and water O-H stretching vibration is a very difficult task. But these bands are distinguished easily from the DFT calculations. The bands appeared at 3480 cm<sup>-1</sup> and 1630 cm<sup>-1</sup> are attributed to hydrogen bonded O-H stretching vibration and the O-H-O in-plane bending, respectively. Generally, the O-H stretching band of carboxylic acid exist as hydrogen bonded dimer but in the present case, the experimental spectrum of the salt suggests that the O-H stretching vibration appeared at lower wave number (3310 cm<sup>-1</sup>) confirms the formation of O5-H5A...O1 intermolecular hydrogen bonding. Moreover, the O-H stretching band appeared at 3631 cm<sup>-1</sup> (calculated) is attributed to the O-H stretching frequency for free carboxylic acid.

**N-H vibrations:** The bands observed at 3380 and 3360 cm<sup>-1</sup> are attributed due to the asymmetric and symmetric stretching vibrational modes of NH<sub>2</sub> (primary amine) in AHPMH. In AHPMH, the nitrogen atom in the primary amines has trigonal pyramidal configuration (almost sp<sup>3</sup>) and these amines are extremely involved in hydrogen bonding interaction than aromatic amines. The calculated N-H stretching band observed at lower wavenumber (3040 cm<sup>-1</sup>) due to the greater degree of hydrogen bonding interaction. The N2-H2A bond shows the highest intensity of 1780 cm<sup>-1</sup> compared to all other N-H bonds enormously red shifted. The N2-H2A-O5 interaction shows D...A distance of 2.85 Å, which apparently indicates its comparatively strong hydrogen bonding behaviour. In the experimental spectrum, the C=N stretching vibrational frequency appeared at 1670 cm<sup>-1</sup> and the N-H bending deformation band at 1610 cm<sup>-1</sup>. The NH<sub>2</sub> out of plane bending vibration appeared at 790 cm<sup>-1</sup> and calculated values are listed in Table-4.

**C-N vibration:** Generally, the C-N stretching vibrations were observed at 1382-1266 cm<sup>-1</sup> region [31]. In present case, protonation appears particularly at imino nitrogen atom (C=NH<sub>2</sub>) and electron density on nitrogen slightly lower than AG imino nitrogen moiety. This clearly established that the C=N stretching vibration intensities of salt is higher than C=N stretching vibrations of AG. The calculated C=N stretching modes were observed at 1681, 1665 and 1657 cm<sup>-1</sup>. Usually, the N-N stretching frequency observed at 980-960 cm<sup>-1</sup> for hydrazine and its derivatives. The N-N stretching vibration frequency of the title compound slightly increased due to the lower bond distance (1.401 Å) and this band appeared at 1130 cm<sup>-1</sup> (bond strength and force constant increases, the value of vibrational frequency increases).

**Mulliken charge analysis:** Mulliken charge analysis has been employed to explain the properties such as polarizability and proton charge transfer in chemical reaction [32,33]. The Mulliken charge distribution was calculated using B3LYP/6-311G(d,p) and graphical representations of atomic charges are shown in Fig. 6. The charge distributions of reactants (AG and phthalic acid) are also calculated for comparison purpose (charge transfer during the reaction). The atomic charge distribution data are given in Table-5.

In aminoguanidine (AG), carbon atom (C1) is comparatively less stable than surrounding nitrogen atoms (N2, N3 and N4), hence the direction of dipoles N-C bonds in the molecule towards nitrogen atom (lone pair). Thus, dipole moment and polar aspects of the N-H bond show greater influence than the N-C bond. The charge distribution on N2, N3 and N4 are -0.4066 e, -0.4323 e and -0.1458 e, respectively. Among these nitrogen atoms, N3 has a large electronegativity than others as well as this atom (N3) act as an excellent proton acceptor. Generally, C-N single bond length is found to be 1.47 Å, the C-N single bond length of many amides, imide and imino appear in the range 1.28-1.39 Å. In AG, the bond lengths of (C1-N2,

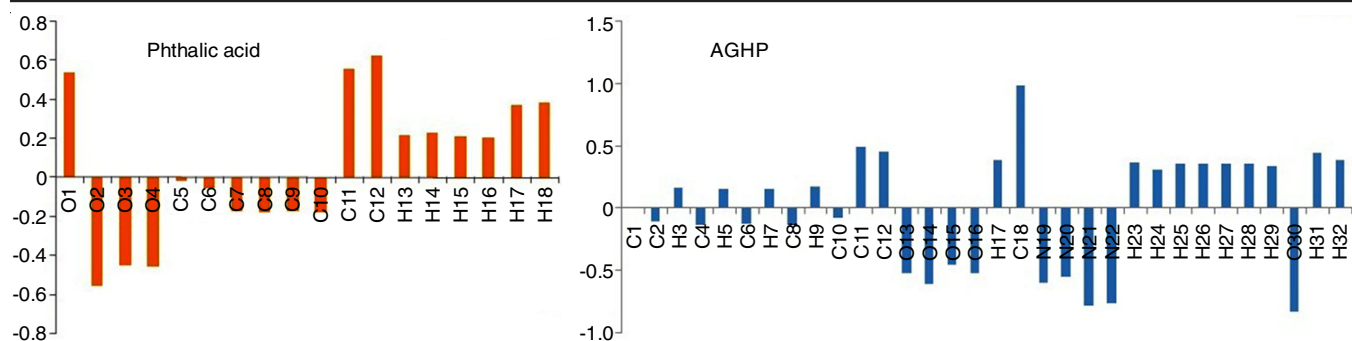


Fig. 6. Mulliken charge distributions

TABLE-5 MULLIKEN CHARGES									
Aminoguanidine (AG)		Phthalic acid			AGHP				
C1	0.070186	O1	0.538558	C10	-0.17938	C1	0.009772	H17	0.384174
N2	-0.4066	O2	-0.55982	C11	0.555641	C2	-0.10557	C18	0.990428
N3	-0.43226	O3	-0.45231	C12	0.627552	H3	0.164244	N19	-0.60653
N4	-0.14583	O4	-0.46129	H13	0.216275	C4	-0.13454	N20	-0.55007
N5	-0.51293	C5	-0.01918	H14	0.227107	H5	0.153845	N21	-0.78494
H6	0.176873	C6	-0.0573	H15	0.208548	C6	-0.1269	N22	-0.76666
H7	0.238667	C7	-0.17621	H16	0.206234	H7	0.154682	H23	0.368541
H8	0.265277	C8	-0.17824	H17	0.372627	C8	-0.1348	H24	0.310642
H9	0.25123	C9	-0.17362	H18	0.381945	H9	0.176351	H25	0.360888
H10	0.241217					C10	-0.0811	H26	0.360275
H11	0.254176					C11	0.492064	H27	0.355285
						C12	0.453992	H28	0.357115
						O13	-0.52311	H29	0.341857
						O14	-0.61228	O30	-0.8347
						O15	-0.45342	H31	0.444624
						O16	-0.52622	H32	0.381612

C1-N4 and C1-N3 are 1.38 Å, 1.40 Å and 1.28 Å, respectively which are almost similar to the bond distance of C=N (double bond). Thus, C1-N2 bond length is intermediate (1.38 Å) between the single bond and double bond lengths means a partial double bond character between the carbon and nitrogen generates a resonance structure (Fig. 7). This partial double bond nature could be due to formation of the  $\pi$ -bond by  $p$ -orbitals. Thus the hybridization of N2 atom is in between  $sp^3$  and  $sp^2$ .

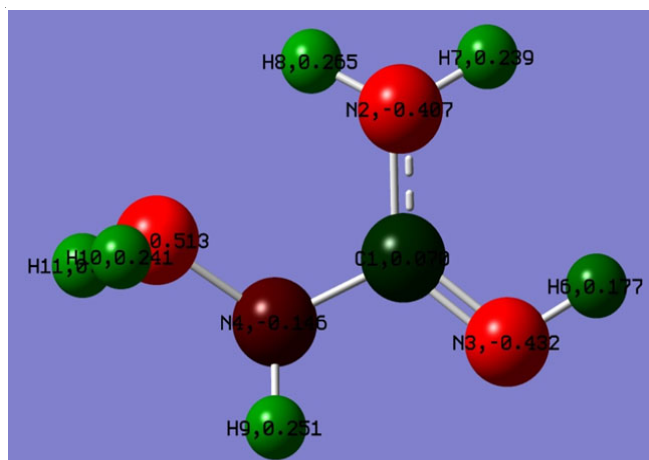


Fig. 7. Partial double bond character between the carbon and nitrogen atom in aminoguanidine(AG)

The  $pK_a$  value plays an important role in proton transfer reaction. Benzene 1,2-dicarboxylic acid (phthalic acid) is a dibasic acid and it acts as a two hydrogen bond donor. The  $pK_a$  values of phthalic acid are 3.89 and 5.51. Thus, the first carboxylic acid easily donates the proton than the second. From Mulliken charge distribution data, the electronegativity difference in C2-carboxylic acid is greater than C1-carboxylic acid. Thus, the difference in electronegativity increases polarization and dipole moment. Hence, the O1-H17 bond is comparatively weaker than O2-H18 and act as a proton donor. Moreover, charge on H1 atom (0.393 e) has slightly more positive than H18 (0.392 e), which also additional support for the removal of proton from C1-carboxylic acid.

**Molecular electrostatic potential (MEP):** Molecular electrostatic potential (MEP) of AG, phthalic acid and AHPMH were carried out to examine electron densities around different atomic environments in the respective molecules. The MEP and counter map of molecules are shown in Fig. 8. The electrostatic potential increased in the order: red < orange < yellow < green < blue. The red colour indicates that the atom with lone pair or negative electrostatic potential which is the site for an electrophilic attack while blue colour indicates the positive electrostatic potential favourable to nucleophilic attack. The electron density counter map shows electron rich red lines are around nitrogen, whereas the electron deficient regions are shown by greenish-yellow lines. In AG, imino nitrogen (N3) has more net

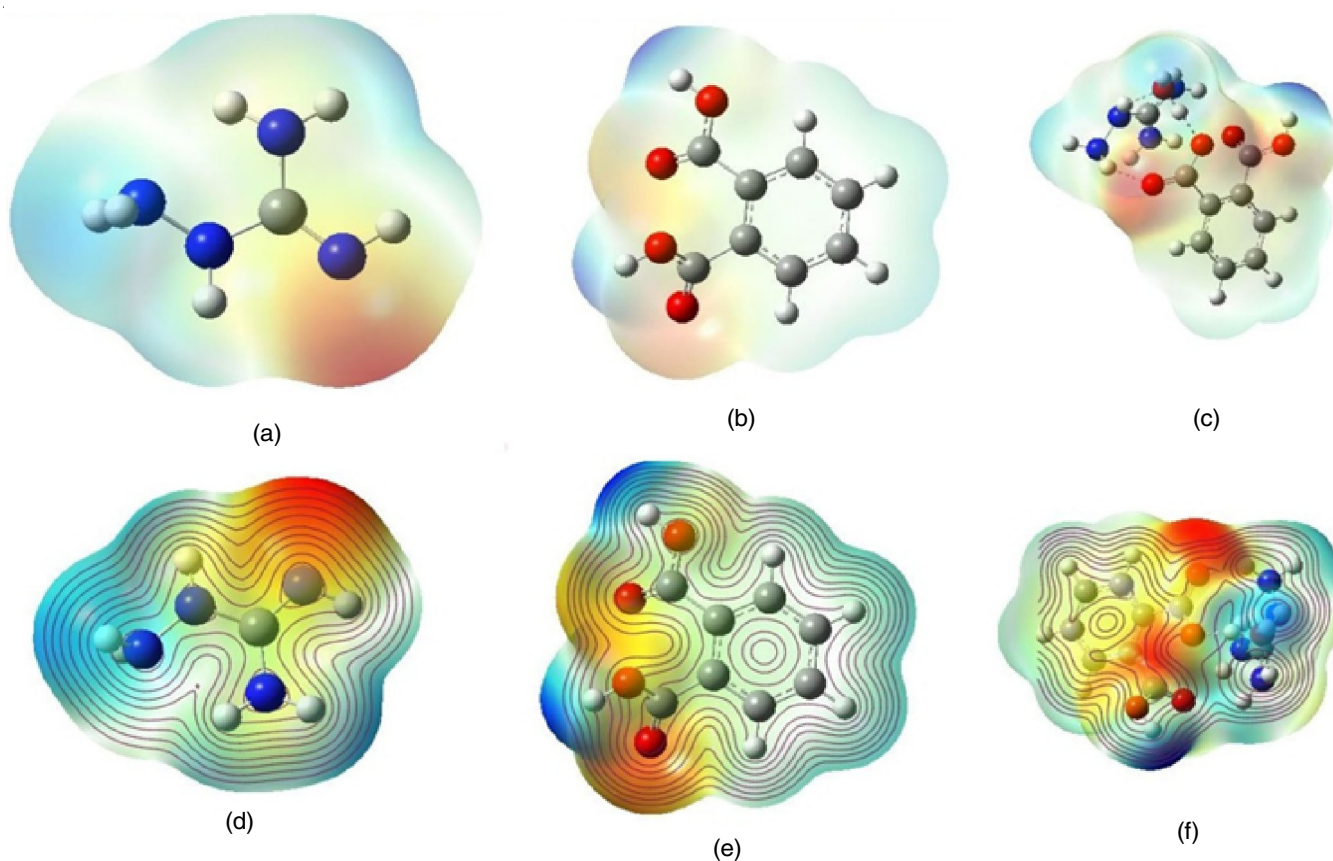


Fig. 8. Electrostatic potential diagram of (a) aminoguanidine(AG); (b) phthalic acid; (c) AHPMH. Below: counter line map of (d) aminoguanidine(AG); (e) phthalic acid (f) AHPMH at B3LYP/6-311+G(d,p) basis level

negative (-0.432 e) character (red) than other nitrogen atoms. In phthalic acid, C1-carboxylic acid is slightly denser blue colour than C2-carboxylic acid hydrogen. Thus, the proton (nucleophile) from C1-carboxylic acid is easily displaced or eliminated and protonates the imino group (electrophile) in AG. Thus the proton ( $H^+$ ) can act as a better electrofuge leaving group. The heterolytic O-H bond cleavage has occurred and remarkable change in charge is observed (-0.6112 e) in carboxylate oxygen (O14) in AHPMH.

**Frontier molecular orbital (FMO) analysis:** The FMO is an effective tool to calculate the global reactivity indices of the molecule such as chemical potential ( $\mu$ ), chemical hardness ( $\eta$ ), electronegativity ( $\chi$ ) and global electrophilicity index ( $\omega$ ). The molecule having a large energy gap is known as a hard molecule and the molecule having a small energy gap is known as a soft molecule. The soft molecules are more polarizable than the hard one because they need small energy for excitation. The HOMO-LUMO energy gap between the reactants and product were calculated (Fig. 9) by B3LYP/6311+G(d,p) basis set. The calculated energy gap values of AG and phthalic acids are 5.98 eV and 5.38 eV, respectively, these values indicate both the reactants are hard species. Usually, soft-soft interactions are only responsible for the formation of covalent pi-bond. In the present case, only hard-hard interaction is taking place and there is no newly formed pi-bond in the product. This also confirms the reactants are not involved in aqueous condensation (amide formation) reaction. The hardness value

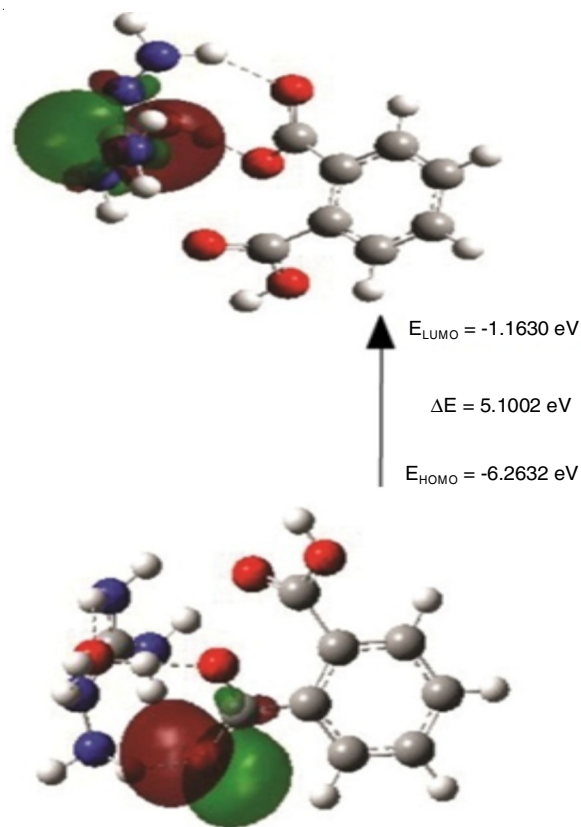


Fig. 9. Frontier molecular orbital energies of AHPMH

of a molecule can be determined by the formula ( $\eta = [-E_{\text{HOMO}} - E_{\text{LUMO}}]/2$ ) [34]. The electro-negativity and electrochemical potential were determined using equations  $\chi = -[E_{\text{HOMO}} + E_{\text{LUMO}}]/2$  and  $\mu = [E_{\text{HOMO}} + E_{\text{LUMO}}]/2$ , respectively. Global electrophilicity is defined as  $\omega = \mu^2/2\eta$ . The calculated energy gap of AHPMH is 6.327 eV. Various global reactivity indices,  $\mu$ ,  $\eta$ ,  $\chi$  and  $\omega$  were found to be -2.550 eV, 3.713 eV, 2.550 eV and 0.875 eV, respectively.

In most acid-base reactions, HOMO-LUMO combinations form new HOMO and LUMO orbitals in the products. In this reaction, the  $a_1$  orbital containing lone pair of electrons of the imino group combines with empty  $1s$ -orbital of the proton ( $\text{H}^+$ ) to form new bonding and antibonding orbitals. The lone pair in the  $a_1$  orbital of imino group is stabilized by this interaction. The interaction of imino group orbitals and one  $\text{H}^+$  orbital gives the eight electrons of  $=\text{NH}_2^+$  ion (formal charge +1). The molecular energy level diagram is shown in Fig. 10.

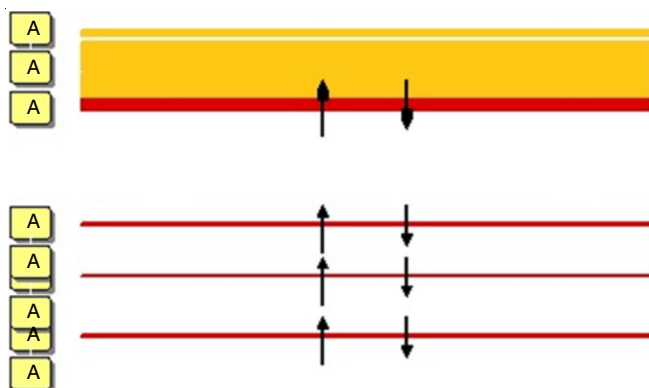


Fig. 10. Energy level diagram of AGHP

**Hirshfeld surface analysis:** Hirshfeld surface analysis [35] is an important tool to study the intermolecular interactions of the crystals. The molecular Hirshfeld surface maps and fingerprint plots were visualized in the crystal Explorer 3.1 program [36,37]. The intermolecular contacts in the crystal packing were mapped using the normalized contacts distance,  $d_{\text{norm}}$ ,  $d_e$  and  $d_i$ , where,  $d_{\text{norm}}$  represents the normalized contact distance,  $d_e$  represents the distance from the point to the nearest nucleus external to the surface and second one is  $d_i$  represents the distance to the nearest nucleus internal to the surface. The analysis was visualized by  $d_{\text{norm}}$  (normalized contact distance), which surface property shows red-white-blue colour scheme [38]. The white surfaces indicates contacts with distances equal to the sum of their vdw radii. Bright red surface indicates intermolecular contacts less than their vdw radii, blue colour indicates the intermolecular contacts longer than their vdw radii.

The normalized contact distance ( $d_{\text{norm}}$ ) map shown in Fig. 11 and red spots show hydrogen bonding contacts. The hydrogen bonds formed between the oxygen atoms (donor) with neighboring oxygen atoms (donor). The 2D representation of fingerprint plots are shown in Fig. 12. The  $\text{H}\cdots\text{H}$  contact exhibits most important contribution (43.6%) to the overall crystal packing (Fig. 12). The  $\text{H}\cdots\text{O}/\text{O}\cdots\text{H}$  interaction show the pair of sharp spikes of  $\text{O}\cdots\text{H}$  ( $\text{N}-\text{H}\cdots\text{O}$ ) and are characterized by strong hydrogen bonding interaction. The crystal property

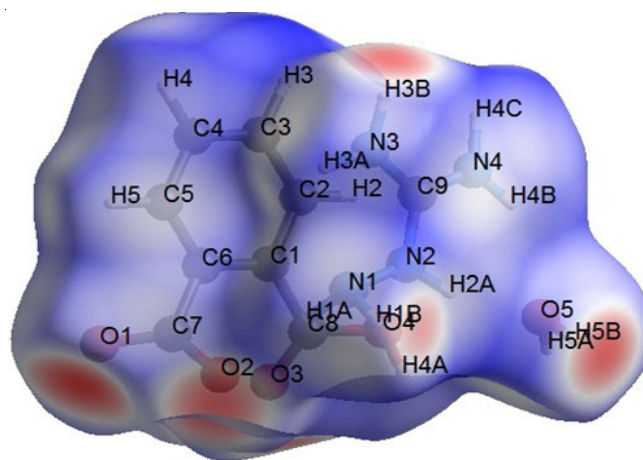


Fig. 11.  $d_{\text{norm}}$  view of the three-dimensional Hirshfeld surface of the title compound

calculation shows that the surface area in the present compound is in the order of  $286.01 \text{ \AA}^2$  and the void to be in the order of  $256.76 \text{ \AA}^3$ .

**Thermal stability analysis:** The thermal stability behaviour of AHPMH was investigated by simultaneous TG-DTA analysis under air flow. The TG-DTA curve of AHPMH is given in Fig. 13. The TG curve shows the compound undergoes multi-step decomposition. In the first step, removal of a lattice water molecule from the crystal lattice takes place with 7% weight loss for which DTA shows an endothermic at  $105 \text{ }^\circ\text{C}$ . The major exothermic decompositions were observed between the temperature range  $200\text{--}600 \text{ }^\circ\text{C}$ . This decomposition temperature range indicates the stability of the salt due to the intermolecular hydrogen bonding interactions [39]. Elimination of  $\text{NH}_3$  molecule through the deamination reaction by the cleavage of N-N bond (exothermic,  $450 \text{ }^\circ\text{C}$ ) takes place leading to the formation of  $\text{NH}_2$  radicals, which continuously abstract H atom from the parent amines giving rise to  $\text{NH}_3$  molecule [35]. Also, the elimination (82.5%) of the gaseous product like  $\text{CO}_2$ ,  $\text{CO}$  and  $\text{CH}_4$  was observed due to the bulk decomposition of the salt. The exothermic peak at  $245 \text{ }^\circ\text{C}$  ascribed to the melting point of the crystal, which extremely in the good agreement with the experimental melting point.

**DNA binding study:** On DNA-ligand interaction (Fig. 14), significant changes were observed in the electronic spectrum of DNA. The hyperchromic shift in the absorption spectrum of DNA is responsible for the ligand's interaction with the double helix of DNA [40]. The hyperchromic shift in the absorption spectrum of DNA was observed in case of electrostatic binding between the ligand and DNA molecule [41,42]. The title compound shows its absorption peak at  $282 \text{ nm}$ , increasing the concentration ( $10 \text{ } \mu\text{M}$ ) of CT-DNA, which exhibits the hyperchromatism with redshift. Eqn. 1 has been used to calculate the binding constant. The value of the binding constant ( $K_b$ ) of the title compound was found to be  $3.15 \times 10^4$ , which indicates that the strong interactions were developed between the title compound and CT-DNA.

$$\frac{[\text{DNA}]}{(\epsilon_a - \epsilon_f)} = \frac{[\text{DNA}]}{(\epsilon_b - \epsilon_f)} + \frac{1}{K_b(\epsilon_b - \epsilon_f)} \quad (1)$$

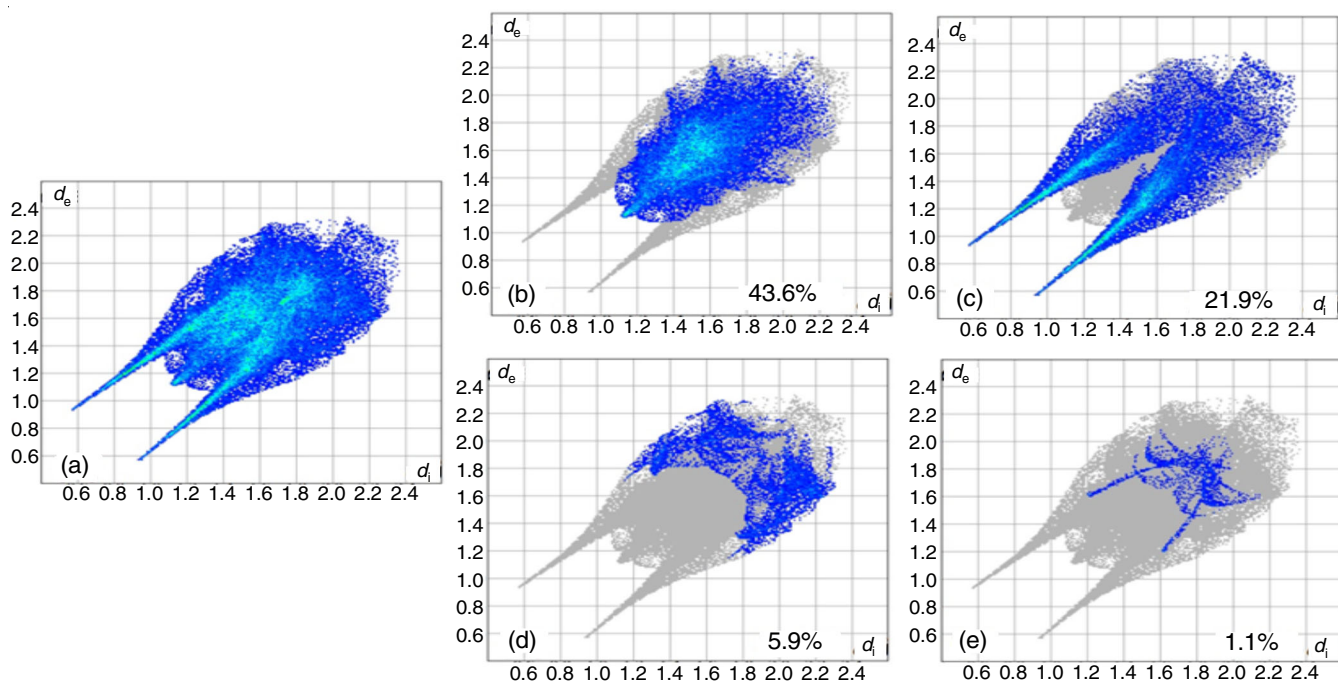


Fig. 12. Two-dimensional fingerprint plots for the title compound, showing (a) all interactions and delineated into (b) H...H (c) H...O/O...H (d) H...C/C...H (e) H...N/N...H

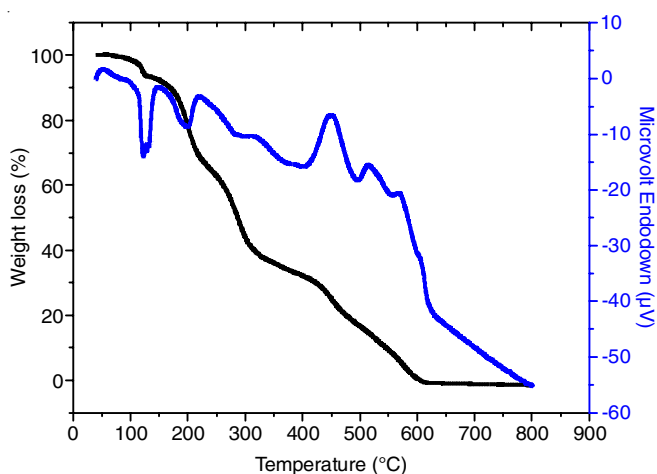


Fig. 13. Simultaneous TG-DTA curve of AHPMH

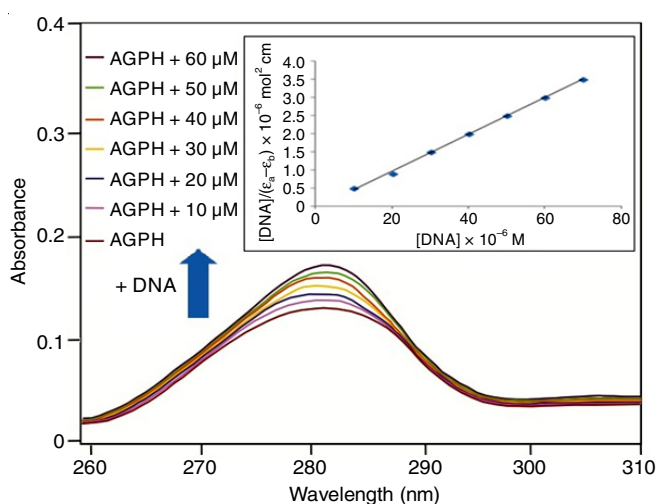


Fig. 14. Absorption spectra of AGPH with different concentration of CT-DNA

**Appendix A. Supplementary material:** Crystallographic data of the compound has been deposited with the Cambridge Crystallographic Data Centre [CCDC No. 2144082]. Data can be obtained at free of charge from [www.ccdc.cam.ac.uk/conts/retrieving.html](http://www.ccdc.cam.ac.uk/conts/retrieving.html) or from the Cambridge Crystallographic Data Centre (CCDC), 12 Union Road, Cambridge CB2 1EZ, UK; fax: +44 01223 336 033; email: [deposit@ccdc.cam.ac.uk](mailto:deposit@ccdc.cam.ac.uk)

#### CONFLICT OF INTEREST

The authors declare that there is no conflict of interests regarding the publication of this article.

#### REFERENCES

- M.R.A. Blomberg and P.E.M. Siegbahn, *Biochim. Biophys. Acta-Bioenerg.*, **1757**, 969 (2006); <https://doi.org/10.1016/j.bbambio.2006.01.002>
- H. Ishikita and K. Saito, *J. R. Soc. Interface*, **11**, 20130518 (2014) <https://doi.org/10.1098/rsif.2013.0518>
- P.H.J. Heller and H.R. Blattmann, *Pure Appl. Chem.*, **36**, 141 (1973); <https://doi.org/10.1351/pac197336010141>
- P. Chou, D. McMorro, T.J. Aartsma and M. Kasha, *J. Phys. Chem.*, **88**, 4596 (1984); <https://doi.org/10.1021/j150664a032>
- M. Scherl, D. Haarer, J. Fischer, A. DeCian, J.-M. Lehn and Y. Eichen, *J. Phys. Chem.*, **100**, 16175 (1996); <https://doi.org/10.1021/jp9609242>
- I. Fernández, P. Hervés and M. Parajó, *J. Phys. Org. Chem.*, **21**, 713 (2008); <https://doi.org/10.1002/poc.1380>
- P. Hervés, R.G. Button and D.L.H. Williams, *J. Chem. Res.*, **234**, 474 (1998); <https://doi.org/10.1039/a803199a>
- R.G.S. Berlinck and S. Romminger, *Nat. Prod. Rep.*, **33**, 456 (2016); <https://doi.org/10.1039/C5NP00108K>
- Y. Kudo, T. Yasumoto, D. Mebs, Y. Cho, K. Konoki and M. Yotsu-Yamashita, *Angew. Chem. Int. Ed.*, **55**, 8728 (2016); <https://doi.org/10.1002/anie.201602971>

10. C.L. Hannon and E.V. Anslyn, Eds.: H. Dugas, *Bioorganic Chemistry Frontiers*, vol. III, Springer: Verlag (1993).
11. S. Patai, *The Chemistry of Amidines and Imidates*, vol. 1, Wiley: Chichester (1975).
12. G. Häfelinger and F.K.H. Kuske, Eds. S. Patai and Z. Rappoport, *The Chemistry of Amidines and Imidates*, John Wiley & Sons, Ltd.; Chichester, UK, pp. 1-100 (1991).
13. E.D. Raczynska, M.K. Cyranski, M. Gutowski, J. Rak, J.-F. Gal, P.-C. Maria, M. Darowska and K. Duczmal, *J. Phys. Org. Chem.*, **16**, 91 (2003); <https://doi.org/10.1002/poc.578>
14. M. Brownlee, *Diabetes Care*, **15**, 1835 (1992); <https://doi.org/10.2337/diacare.15.12.1835>
15. T.M. Osicka, Y. Yu, V. Lee, S. Panagiotopoulos, B.E. Kemp and G. Jerums, *Clin. Sci.*, **100**, 249 (2001); <https://doi.org/10.1042/CS20000194>
16. K. Karjalainen, R. Pasqualini, J.E. Cortes, S.M. Kornblau, B. Lichtiger, S. O'Brien, H.M. Kantarjian, R.L. Sidman, W. Arap and E. Koivunen, *Cancer*, **120**, 589 (2014); <https://doi.org/10.1002/cncr.28419>
17. E.F. Caldin, *J. Chem. Soc.*, **64**, 3345 (1959); <https://doi.org/10.1039/jr9590003345>
18. C.D. Ritchie and R.E. Uschold, *J. Am. Chem. Soc.*, **90**, 3415 (1968); <https://doi.org/10.1021/ja01015a022>
19. C.F. Bernasconi, *Pure Appl. Chem.*, **54**, 2335 (1982); <https://doi.org/10.1351/pac198254122335>
20. D. Peeters, G. Leroy and C. Wilante, *J. Mol. Struct.*, **416**, 21 (1997); [https://doi.org/10.1016/S0022-2860\(97\)00047-1](https://doi.org/10.1016/S0022-2860(97)00047-1)
21. Bruker, APEX2 and SAINT-Plus, Bruker AXS Inc., Madison (2004).
22. A. Altomare, G. Cascarano, C. Giacovazzo and A.J. Guagliardi, *J. Appl. Cryst.*, **26**, 343 (1993); <https://doi.org/10.1107/S0021889892010331>
23. C.K. Johnson, ORTEP ORNL-3794, Oak Ridge National Laboratory, Tennessee (1976).
24. G.M. Sheldrick, SHELXL-2014 Programs for Crystal Structure Determination, University of Cambridge, England (1977).
25. M.J. Frisch, G.W. Trucks, H.B. Schlegel, G.E. Scuseria, M.A. Robb, J.R. Cheeseman, G. Scalmani, V. Barone, G.A. Petersson, H. Nakatsuji, X. Li, M. Caricato, A.V. Marenich, J. Bloino, B.G. Janesko, R. Gomperts, B. Mennucci, H.P. Hratchian, J.V. Ortiz, A.F. Izmaylov, J.L. Sonnenberg, D. Williams-Young, F. Ding, F. Lipparini, F. Egidi, J. Goings, B. Peng, A. Petrone, T. Henderson, D. Ranasinghe, V.G. Zakrzewski, J. Gao, N. Rega, G. Zheng, W. Liang, M. Hada, M. Ehara, K. Toyota, R. Fukuda, J. Hasegawa, M. Ishida, T. Nakajima, Y. Honda, O. Kitao, H. Nakai, T. Vreven, K. Throssell, J.A. Montgomery, J.E. Peralta Jr., F. Ogliaro, M.J. Bearpark, J.J. Heyd, E.N. Brothers, K.N. Kudin, V.N. Staroverov, T.A. Keith, R. Kobayashi, J. Normand, K. Raghavachari, A.P. Rendell, J.C. Burant, S.S. Iyengar, J. Tomasi, M. Cossi, J.M. Millam, M. Klene, C. Adamo, R. Cammi, J.W. Ochterski, R.L. Martin, K. Morokuma, O. Farkas, J.B. Foresman and D.J. Fox, *Gaussian 16*, Revision A.03; Gaussian, Inc., Wallingford CT (2016).
26. A.D. Becke, *Phys. Rev. A Gen. Phys.*, **38**, 3098 (1988); <https://doi.org/10.1103/PhysRevA.38.3098>
27. A.D. Becke, *J. Chem. Phys.*, **98**, 5648 (1993); <https://doi.org/10.1063/1.464913>
28. A.G. Baboul, L.A. Curtiss, P.C. Redfern and K. Raghavachari, *J. Chem. Phys.*, **110**, 7650 (1999); <https://doi.org/10.1063/1.478676>
29. R.G. Parr and W. Yang, *Density Functional Theory of Atoms and Molecular Orbital Theory*, Oxford University Press, New York (1998).
30. G. Varsanyi, *Assignments of Vibrational Spectra of 700 Benzene Derivatives*, Wiley: New York (1974).
31. V. Krishnakumar and N. Prabavathi, *Spectrochim. Acta A Mol. Biomol. Spectrosc.*, **72**, 743 (2009); <https://doi.org/10.1016/j.saa.2008.11.012>
32. K. Jug and Z.B. Maksic, *Theoretical Model of Chemical Bonding*, Springer: Berlin (1991).
33. S. Fliszar, *Charge Distributions and Chemical Effects*, Springer, Berlin, Heidelberg: New York (1983).
34. S.K. Kurtz and T.T. Perry, *J. Appl. Phys.*, **39**, 3798 (1968); <https://doi.org/10.1063/1.1656857>
35. M.A. Spackman and D. Jayatilaka, *CrystEngComm*, **11**, 19 (2009); <https://doi.org/10.1039/B818330A>
36. M.A. Spackman and J.J. McKinnon, *CrystEngComm*, **4**, 378 (2002); <https://doi.org/10.1039/B203191B>
37. A.L. Rohl, M. Moret, W. Kaminsky, K. Claborn, J.J. McKinnon and B. Kahr, *Cryst. Growth Des.*, **8**, 4517 (2008); <https://doi.org/10.1021/cg8005212>
38. D. Cremer, *Acta Crystallogr. B*, **40**, 498 (1984); <https://doi.org/10.1107/S0108768184002548>
39. S.R. Naidu, K.V. Prabhakaran, N.M. Bhide and E.M. Kurian, *J. Therm. Anal. Calorim.*, **61**, 861 (2000); <https://doi.org/10.1023/A:1010113707251>
40. Ö. Karaca, S.M. Meier-Menches, A. Casini and F.E. Kuhn, *Chem. Commun.*, **53**, 8249 (2017); <https://doi.org/10.1039/C7CC03074F>
41. D. He, L. Wang, L. Wang, X. Li and Y. Xu, *J. Photochem. Photobiol. B*, **166**, 333 (2017); <https://doi.org/10.1016/j.jphotobiol.2016.12.003>
42. J.H. Shi, Y.Y. Lou, K.L. Zhou and D.-Q. Pan, *J. Biomol. Struct. Dyn.*, **36**, 2738 (2018); <https://doi.org/10.1080/07391102.2017.1365012>